Multi-Physics Optimization of High Power Density Induction Machines for Railway Traction Drives

J. Buschbeck, M. A. Vogelsberger*, A. Orellano
Bombardier Transportation GmbH
Am Rathenaupark, 16761 Hennigsdorf, Germany
*Bombardier Transportation Austria GmbH
Hermann-Gebauer-Straße 5, 1220 Vienna, Austria

E. Schmidt, M. Bazant**
Vienna University of Technology, Inst. of Energy Systems and Elect. Drives, Gußhausstraße 25, 1040 Vienna, Austria
**Bombardier Transportation (Switzerland) Ltd.
Brown Boveri-Straße 5, 8050 Zurich, Switzerland

***Abstract* — This paper applies a multi-physics optimization exemplary considering electromagnetic and aero-/ thermo-dynamic performance. Today, electrical drives used for railway traction face limited space constrains which leads to high power density machines. That requires advanced cooling concepts that are able to highly effectively discharge heat without adding more volume and weight in the boggy. A novel optimization approach for internal forced air-cooled traction drives will be presented. The optimization method integrates multi-physic performance evaluations. As an example, here, the coupling of aero- and thermodynamic cooling performance with electromagnetic performance evaluation is presented. However, the method is made to be easily extended to consider additional physics e.g. material strength or acoustic objectives, production cost functions or additional limiting constraints. FEA (finite element analysis) is used for obtaining electromagnetic properties whether analytical code is used to rate the amount of heat discharged by the cooling fluid. The aero-/ thermodynamic performance of the optimized solution is finally validated by full CFD (computational fluid dynamics) with conjugate heat transfer.**

Keywords* — *AC motor drives, design optimization, finite element analysis, induction machines, multi-physics, thermal management of electronics, traction motors

I. INTRODUCTION

In railway traction drive applications the installation space is limited e.g. by traction gauge while an increase in machine power is desired. That leads to much higher electromagnetic and thermal utilization in comparison to standard industrial variable speed drives. The thermal utilization is restricted by limited temperature resistance of the insulation materials used. Consequently, an optimization with respect to a maximum electromagnetic performance and thermal limitations will be carried out. Here, aspects of electromagnetic, thermal and mechanical loadabilities and the characteristics of these machines, in particular torque density and stray field inductances, have to be taken into account with the multi-physics optimization.

II. LOADABILITY ASPECTS

The optimization must consider fundamental aspects of electromagnetic, thermal and mechanical loadabilities.

First, the dimension of induction machines is defined by χ, the ratio of stacking length l_i and pole pitch τ_p. It depends on the number of pole pairs p and lies within a typical range of

$$\chi = \frac{l_i}{\tau_p} = (1 \dots 2)\sqrt[3]{p}\,. \tag{1}$$

Therefore, typical lengths of induction machines can be assumed to be variable over a length scale λ such as stacking length l_i and air-gap diameter D_i [1].

A. Mechanical Loadability

As stated in [1], the maximum speed n_{max} of an induction machine becomes inversely proportional to the length scale λ,

$$n_{max} \sim \lambda^{-1}\,. \tag{2}$$

This also holds for the maximum supply frequency f_{max}, since synchronous rotor speed and stator frequency are proportional,

$$f_{max} \sim \lambda^{-1}\,. \tag{3}$$

B. Thermal Loadability

In general, the stationary temperature rise ΔT of an electrical machine caused by any losses P_L follows from

$$\Delta T \sim \frac{P_L}{A_T}\,, \quad A_T \sim \lambda^2\,, \tag{4}$$

where the cooling surface A_T depends quadratically on the length scale λ.

C. Electric Loadability

The power losses of any winding P_{Cu} can be expressed with current density J and conductor volume λ^3,

978-1-4799-7800-7/15/$31.00 ©2015 IEEE

$$P_{Cu} \sim J^2\,\lambda^3\,. \tag{5}$$

The temperature rise caused by such losses is directly proportional to the product of the RMS value of the current sheet of the armature winding A and the current density J of the winding conductors,

$$\Delta T \sim \frac{P_{Cu}}{A_T} \sim A\,J\,, \tag{6}$$

which is independent of the scale of an electrical machine (1) and (2), [2]. Thus, with respect to temperature rise and consequently cooling methods the product $A \cdot J$ is one of the most important design criteria.

D. Magnetic Loadability

Thereby, magnetic flux density B_δ within the air-gap and supply frequency f determine the hysteresis losses $P_{Fe,Hy}$ and eddy current losses $P_{Fe,EC}$ within the laminated iron as given by

$$P_{Fe,Hy} \sim f\,B_\delta^2\,\lambda^3, \quad P_{Fe,EC} \sim f^2\,B_\delta^2\,\lambda^3\,. \tag{7}$$

With the constant field region, the hysteresis losses are more significant at lower speeds. On the one hand, the eddy current losses will become more interesting with higher speeds. On the other hand, in the field weakening range with $B_\delta\,f \approx \text{const}$, these losses are rather decreasing or constant.

E. Torque Density

The well-known Esson utilization number $C_{IM} = \pi^2\,\tau_\delta$ defines the apparent power S_{IM} of an induction machine in dependence on air-gap diameter D_i, stacking length l_i and synchronous speed n_s as given by

$$S_{IM} = C_{IM}\,D_i^2\,l_i\,n_s\,. \tag{8}$$

However, the apparent torque T_{IM} of the induction machine follows from

$$T_{IM} = \frac{S_{IM}}{2\,\pi\,n_s} = 2\,\tau_\delta\,V_\delta\,, \tag{9}$$

and is proportional to the product of tangential stress τ_δ and volume

$$V_\delta = \frac{\pi}{4}\,D_i^2\,l_i \sim \lambda^3\,. \tag{10}$$

The maximum average tangential stress τ_δ within the air-gap of an induction machine is given by

$$\tau_\delta = \frac{1}{\sqrt{2}}\xi_1\,A\,B_\delta\,, \tag{11}$$

where B_δ is the magnitude of the fundamental wave of the radial component of the magnetic flux density within the air-gap and ξ_1 is the total winding factor including pitch, distribution and, if applicable, skewing terms.

F. Stray Field Inductances

Typically, the most important portion of the stray field inductances arises from stator and rotor slots. The normalized values of these stray field inductances are proportional to the stray coefficient of the slots λ_σ and can be written as

$$l_\sigma \sim \lambda_\sigma \frac{A}{B_\delta}\,. \tag{12}$$

Consequently, these inductances depend on current sheet A and air-gap flux density B_δ. It should be noted, that the stray coefficient λ_σ is proportional to the slot height to width ratio.

In order to achieve a high field weakening capability of the induction machine, the torque characteristic must provide a ratio of maximum torque to nominal load torque as the factor of the desired field weakening range. Therefore, the stray field inductances must not change significantly when starting from an initial design which fulfills the criteria of the application.

G. Summary

By keeping electric as well as magnetic utilization constant, the losses of an induction machine (5) and (7) grow with the third of the length scale. However, the cooling surface grows only to the square of the scale. As a consequence, an increased scale of an electrical machine yields more and more importance for the cooling methods.

Assuming a given temperature rise due to the rather load-independent iron losses, the magnetic flux density can vary in the range of

$$B_\delta \sim \lambda^{0.5} \ldots \lambda\,. \tag{13}$$

As given above, the stray field inductances should be kept constant.

$$A \sim B_\delta \sim \lambda^{0.5} \ldots \lambda\,. \tag{14}$$

Therefore, the maximum average tangential stress depends on the scale as given by

$$\tau_\delta \sim \lambda \ldots \lambda^2 \tag{15}$$

and the maximum torque T_{IM} of an induction machine (9) grows with the scale as of

$$T_{IM} \sim \lambda^4 \ldots \lambda^5\,. \tag{16}$$

However, an increasing armature current sheet A asks for a decreasing current density J within the windings. But the stray field inductances restrict rather to a constant current density. Furthermore, as given by (6), the cooling of the load-dependent losses asks for efficient cooling methods additionally [3, 4].

III. Model Electromagnetics

A. Finite Element Methode

Commercial finite element software is widely available for structural mechanics, thermodynamics as well as electro-

magnetics. Nowadays, even multi-physics approaches with a strong coupling of the different physical domains exist which carry out a simultaneous setup and solution of the problem. Since the optimization algorithm discussed later is rather a sequential one, weak coupled finite element analyses of the different physical domains are carried out instead. Since in particular with electrical machines very different finite element discretizations are necessary between electro-magnetics and thermodynamics, the sequential solution of these domains is preferable and advantageous. With such an approach, we can also incorporate analytical methods additionally.

In general, the finite element method is highly accurate for integral quantities like in particular for electromagnetics such as inductances and power losses. On the other hand, the quantities obtained from local values depend strongly on the discretization. For electromagnetics, this holds particularly for the evolved electromagnetic torque and the iron losses. Both quantities are evaluated from local magnetic densities, the first one inside the air-gap, the latter ones within the various iron regions. Thus, the possibility of using different finite meshes between the domains will be confirmed.

With regard to the rotation of electrical machines with the electromagnetics solutions, it is state of the art to utilize optimized modeling and if possible also solving strategies. They keep fixed meshes of stator as well as rotor and only deal with the air-gap region to represent the rotation. Thus, the numerical accuracy is kept constant for all analyses. [5]

B. Adapted Code

Company internal formulae are integrated to predict losses agreeing well with measurements. Coefficients $a - d$ in (17) and (18) are chosen in such a way to match measured iron losses in yoke sheet area dP_y and teeth sheet area dP_t. v_{10} is the sheet loss coefficient for used sheet type.

$$dP_y = a \cdot B_y^2 \cdot v_{10} \left(\frac{f}{50}\right)^b \tag{17}$$

$$dP_t = c \cdot B_t^2 \cdot v_{10} \left(\frac{f}{50}\right)^d \tag{18}$$

C. Validation

To validate the accuracy of FEA predicted losses measurements were performed. Table 1 shows good agreement within an error range of 15 %.

TABLE 1: COMPARISON MEASSURED AND SIMULATED IRON LOSSES.

Voltage [V]	Measured Iron Losses [W]	FE Simulated Iron Losses [W]	Deviation [%]
800	1 200	1 162	-3.2
1400	3 100	3 550	14.5
1800	6 200	5 827	-6.0

IV. OPTIMIZATION STRATEGY

Different cooling duct configurations are investigated where cooling air passes axially through stator and rotor iron stack. Cooling ducts can be arranged in whole iron yoke areas, see Fig. 1.

The optimization evaluates both the electromagnetic performance as well as the iron stack temperature required for heat removal. The two evaluations are one way coupled; within the electromagnetic calculation the heat sources for the thermal analysis are determined

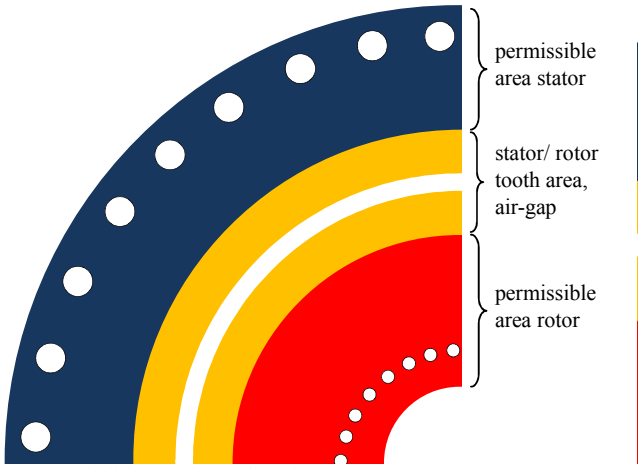

Fig. 1: Permissible area for cooling ducts.

Fig. 2 shows the optimization loop. Each step is described in the following subsections.

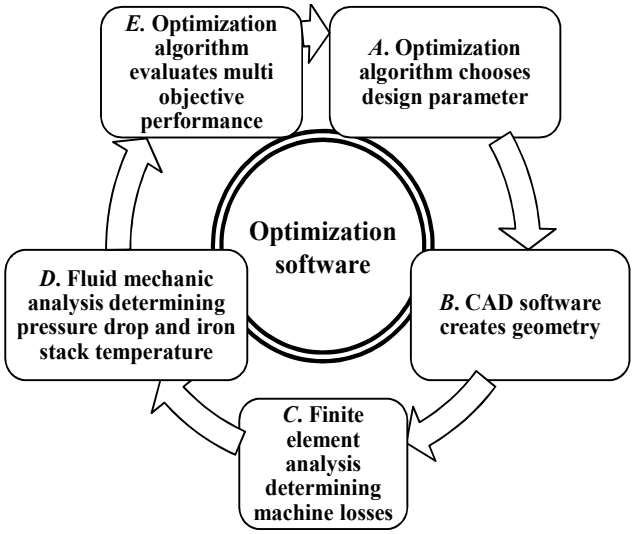

Fig. 2: Optimization loop.

A. Parameters

There are parameters present modifying the shape of the ducts and some define the flow properties. The geometric parameters are defined as scaled quantities to allow easy application of the method to machines of different dimensions. The parameters are the following:

- *Duct position*: Defines radial distance from center point. Scaled to the radial dimension of the yoke area in rotor and stator, respectively.

- *Duct top width*: Defines length of upper edge absolutely.
- *Duct bottom width*: Defines length of lower edge in relation to upper edge. Setting it to minimal value results in triangular shape.
- *Duct height*: Defines duct height in respect to radial dimension of the yoke.
- *Duct top/bottom radius*: Defines radii of top and bottom vertices in relation to maximum possible radius, respectively. These parameters can result in fully circular shaped ducts.
- *Flow distribution*: Defines volume flow distribution between stator and rotor ducts.
- *Pressure target*: Defines the target overall pressure drop. The volume flow is then given with the associated value from the fan curve.

The number of stator and rotor ducts results to fulfill the last two parameters. Fig. 3 shows exemplary the possible variation of the geometry.

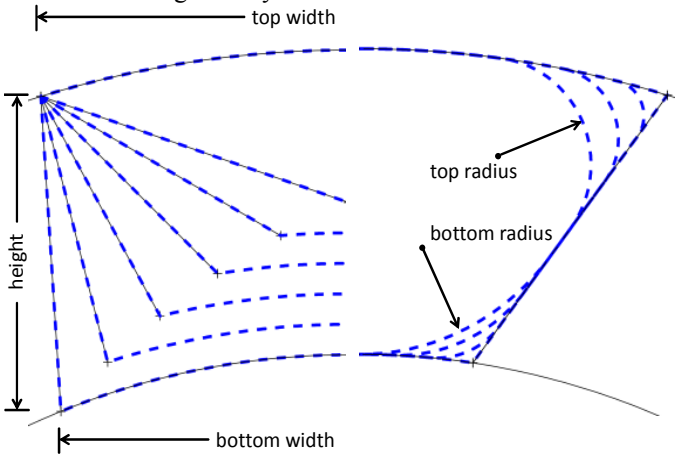

Fig. 3. Variation in: left) duct height and lower edge length in respect to upper edge, respectively; right: upper and lower radius.

The workflow is structured in three parts: First, the shape of the ducts is constructed converting the parameters to geometric quantities. Next, the area and circumference of the ducts are calculated. Then, the duct numbers can be obtained in such a way to fulfill the pressure and flow distribution constraints. Analytical formulae are used to calculate the flow state which is described in detail in [6].

The parameter influence was investigated performing a sensitivity analysis. Parameters without significant impact on the objectives were set to constant to speed up optimization time with reducing the number of required design evaluations by doing so.

B. Geometry Creation

The CAD software is able to allocate every design input to a parameter. The challenge was to find an implementation to automatically consider possible asymmetric contour of the stator lamination. Fig. 4 shows the three possible solutions that can be handled: a) with chosen position no intersection occurs, b) ducting must consider asymmetry, c) regular duct distribution does not lead to intersection. After geometry creation, a 2D geometry is exported for the FEA whereas the CFD needs a full 3D model.

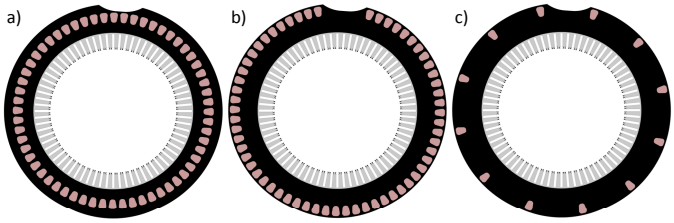

Fig. 4: Compensation of asymmetry; a) and c) no compensation required.

C. Electromagnetic Evaluation

The electromagnetic evaluation is automated by a script driven finite element analysis.

Preprocessing: First, the geometry is imported and the predefined mesh settings are applied, physic quantity definitions like material properties, supply voltage sources, etc. are loaded.

Solving: Two cases are calculated. To obtain magnetizing current and average flux densities in tooth and yoke region, no-load operation is simulated. In a second run, the load case defines iron losses as well as resistive losses.

Open source MUMPS[1] is used, a direct solver capable of utilizing parallelization. The advantage here is that the solver can allocate its own memory in addition to reserved memory by the software [7]. Then, solving parameters like precision, iteration number and relaxation factor are defined and the two solving scenarios 'load case' and 'no-load case' are set up.

Postprocessing: After performed calculation the needed output values are computed. To consider additional losses e.g. due to the deterioration of the sheet permeability after the stamping process, company's internal equations for loss prediction are used to obtain values closer to measurements performed before, see section III.B.

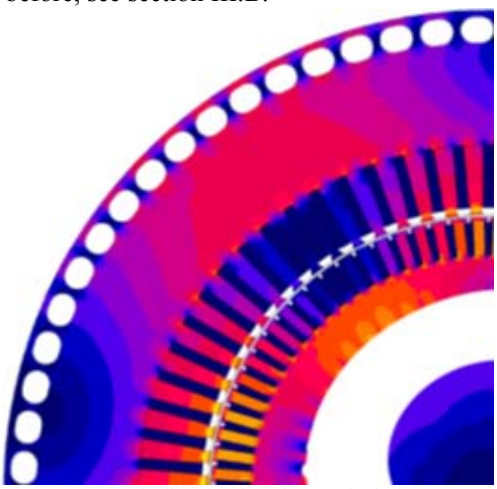

Fig. 5: Instantaneous magnetic flux density of example design.

[1] Multifrontal Massively Parallel sparse direct Solver, see http://mumps.enseeiht.fr.

The magnetic flux distribution is shown in Fig. 5of an example design created by the optimization software.

D. Fluid Mechanical Analysis

The fluid mechanical analysis is performed analytically. First, the pressure loss is determined using pipe pressure drop coefficients from [8]. Second, the heat transfer coefficient is obtained with an empirical approach to calculate the Nusselt number. Then, the surface temperature is iterated until steady state is reached and discharged energy is equal to the loss heat source terms. The analytical model used is described in [6].

E. Optimization Algorithm

Optimization algorithms must choose designs in a way the optimum is reached with minimal design evaluations required. For this purpose the group of evolutionary algorithms mimic the natural selection process. In this analogy, a single gene is equivalent to a parameter, a chromosome to one design and the design space is equivalent to the whole population.

To create new designs the Multi-Objective Genetic Algorithm (MOGA-II) is used applying the following mechanisms [9]:

- Crossover interchanges sections of the chromosomes of parent designs with a certain probability.
- Mutation modifies a single gene, and the mutation ration defines hereby the percentage of modified genes.
- Selection and elitism ensures the preservation of best designs in the population [10].

V. Optimization Results

With optimizing for objectives motor temperature and electromagnetic performance represented by magnetizing current a 2D plot can be made for visualization with averaging rotor and stator temperatures. A set of optimal solutions in respect of both objectives form the so called Pareto optimal[2], see Fig. 6 most of the orange line. One example design from the Pareto set is chosen to quantify performance improvements. However, it must be clear that another solution behaves better in respect to one objective with a trade-off of the other.

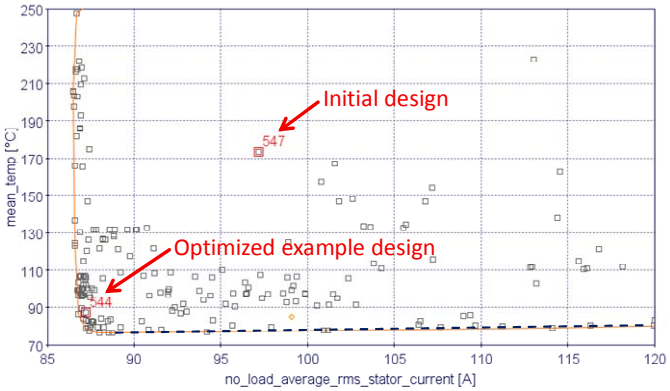

Fig. 6: Plot mean temperature vs. magnetizing current.

[2] named after Italian economist Vilfredo Pareto (1848-1923) and labels a state where it is not possible to improve one objective without deteriorating the other.

A. Optimized Design Performance

For the chosen example design from the Pareto curve both objectives could be improved. The magnetization current could be reduced about -10.2□% for constant mechanical output power and the losses could be reduced up to -9.3□%. Hence, the reduction of total losses counts -1.5□%. Detailed changes in the iron and resistive losses are given in Table 2.

TABLE 2: VARIATION IN OPTIMIZED DESIGN LOSSES OF INITIAL DESIGN.

Rotor	Iron losses	-9.3 %
	Resistive losses	-1.4 %
	Sum	-1.4 %
Stator	Iron losses	+1.3 %
	Resistive losses	-2.4 %
	Sum	-1.5 %
Sum Motor		-1.5 %

For evaluating the cooling performance full CFD calculations including conjugate heat transfer were realized. Commercial CFD code was used, however, here it is only assumed that the method is consistent in itself. A significant temperature reduction up to -15□K could be achieved, see Fig. 7 for a comparison of the temperature distributions. The temperatures in the iron stack are not distributed rotation symmetrical caused by not symmetrical stator yoke radial length. It is the source of a local temperature peak of about 10□K and even continues to the downstream winding head. The cooling flow is directed from left to right and exits there.

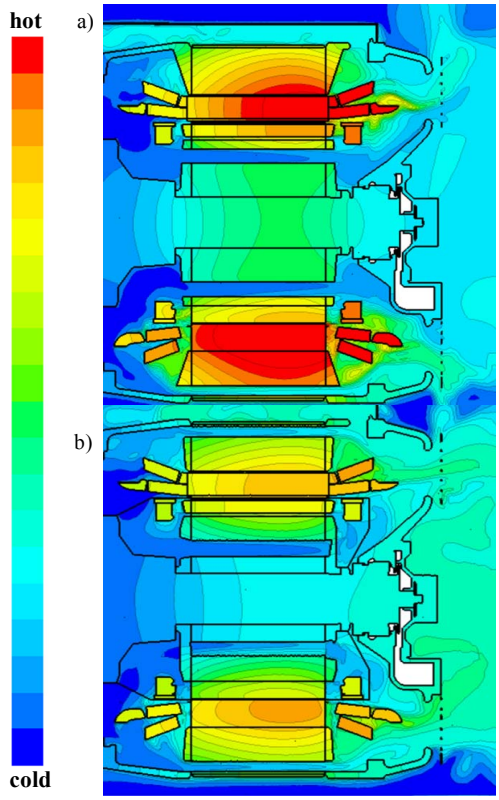

Fig. 7: Cross section CFD heat distribution; a) initial design, b) optimized design.

The reason of rising iron stack temperatures in axial/

downstream direction is decreasing temperature difference caused by increasing fluid temperature. It needs to be taken care of a sufficient temperature difference in the region of downstream winding head to ensure enough cooling. As it can be seen in the temperature plots as well the average fluid outflow temperature is higher for the optimized example design. That is the result of reducing the volume flow rate and allowing higher pressure drop while keeping the fan power constant.

B. Results Utilization

In railway application electrical machines must be fully thermally utilized. Therefore different scenarios were investigated how to use the increased heat transfer all based on the temperature level of the initial machine which must not be exceeded.

1) Increase in power density

The maximum possible increase in power density without exceeding initial machine temperature was done by iterating the electrical losses as heat sources in CFD. Thereby, the loss distribution was assumed to be constant. In the next step FEA mechanical output power was increased until the losses equate the iterated heat sources. Due to lower efficiency of higher thermally utilized machine the increase in output power of about 8.6□% is lower than the increase of discharged heat of about 15.3□%.

2) Reduction in volume flow, fan power and fan noise

As well with iteration within CFD the volume flow was reduced until initial motor temperature is met. Up to -15.6□% less volume flow is required. Caused by the decreased pressure drop for less volume flow the external fan consumes about -39.1□% less power assuming same fan efficiency in new operation point.

The decreased volume flow can be realized by reducing the number of revolutions per time of the fan. Audible fan noise approximation in [11] gives reduced sound pressure level of about -3.7□dB(A).

VI. Conclusion

A new approach for multi-physics optimization of induction machines operated in railway traction drives has been presented. The proposed method can very effectively combine numerous performance evaluation tools. Here, tools from electromagnetic FE calculation and aero-/thermodynamic calculation were used. The presented results show that huge potential can be utilized for both objectives motor temperature and magnetizing current. It could be shown that the magnetization current could be reduced about -10.2□% for constant mechanical output power. Validation of the results with CFD showed that motor temperature can be decreased drastically or power density can be increased with not exceeding the same thermal utilization of the initial machine. The better cooling design as well allows reduction in cooling flow which reduces fan power and audible fan noise.

Acknowledgment

The authors want to thank Bombardier Transportation - PPC Drives Development Center1-Vienna especially the electrical calculation group/ mechanical design group (head Mr. Harasleben; Mr. Sieder) for their generous support. Special thanks go to Bombardier Transportation - Centre of Competence (CoC) Aero- and Thermodynamics in Hennigsdorf (head Mr. Goelz; Mr. Martens and Mr. Mauss) for numerous computation hours, outstanding support and valuable feedback. Special thanks from the authors also go to Mr. Baro for R&D funding and the great support.

References

[1] J. Pyrhönen, T. Jokinen and V. Hrabovcová, Design of Rotating Electrical Machines, John Wiley & Sons Ltd, 2008.

[2] M. Islam, H. Khang, A. Repo and A. Arkkio, "Eddy Current Loss and Temperature Rise in the Form-Wound Stator Winding of an Inverter Fed Cage Induction Motor," *IEEE Trans. on Magnetics,* vol. 46, no. 8, August 2010.

[3] H. Gorginpour, H. Oraee and R. McMahon, "Electro-magnetic-Thermal Design Optimization of the Brushless Doubly Fed Induction Generator," *IEEE Trans. Industrial Electronics,* vol. 61, no. 4, pp. 1710 - 1721, 2014.

[4] Z. Yujiao Zhang, R. Jiangjun, H. Tao, Y. Xiaoping, Z. Houquan and Y. Gao, "Calculation of Temperature Rise in Air-cooled Induction Motors Through 3-D Coupled Electromagnetic Fluid-Dynamical and Thermal Finite-Element Analysis," *IEEE Trans. on Magnetics,* vol. 48, no. 2, pp. 1047 - 1050, August 2012.

[5] E. Schmidt, "Finite Element Analysis of Electrical Machines and Transformers - State of the Art and Future Trends," *International Journal for Computation and Mathematics in Electrical,* vol. 30, no. 06, 2011.

[6] J. Buschbeck, M. A. Vogelsberger, A. Orellano and E. Schmidt, "Aspects of Electromagnetic-Thermal Coupled Optimization of Asynchronous Machines for Traction Drives," *ICEM conference proceedings,* pp. 2152-2157, 09 2014.

[7] CEDRAT, "User Guide Flux 11," Meylan, France, 2012.

[8] VDI-Gesellschaft Verfahrenstechnik, VDI Heat Atlas, 2nd ed., V. D. Ingenieure, Ed., Berlin: Springer, 2010.

[9] N. Gould, An Introduction to Angorithms for Countinuous Optimization, Laboratory, Oxford University Computiong Laboratory and Rutherford Appleton, 2006.

[10] C. Reeves and J. Rowe, "Genetic Algorithms - Principles and Perspectives: A Guide to GA Theory," *Operation Research/ Computer Science Interfaces Series,* vol. 20, 2003.

[11] C. Harris, Handbook of acoustical measurements and noise control, New York: McGraw-Hill, 1991.